Electronic Supplementary Material (ESI) for ChemComm.

Supporting Information

PDDA Induced Step-Pyramidal Shaped Nickel-Platinum (Ni-Pt) Nanoparticles for Enhanced 4-Nitrophenol Reduction

Lourdes Bazán-Díaz,[a] Ariadna Pérez,[a] Naveen Kumar Reddy Bogireddy,[b] J. Jesús Velázquez-Salazar,[c] Israel Betancourt-Reyes,[a] Miguel José-Yacamán,[a,c] Raúl Herrera-Becerra,[b] and Rubén Mendoza-Cruz*[a]

[a] Instituto de Investigaciones en Materiales, Universidad Nacional Autónoma de México (UNAM). Circuito Exterior, Ciudad Universitaria, Ciudad de México, 04510, México.

[b] Instituto de Física, Universidad Nacional Autónoma de México (UNAM). Circuito de la Investigación Científica, Ciudad Universitaria, Ciudad de México, 04510, México.

[c] Applied Physics and Materials Science Department and Center for Material Interfaces Research and Applications (MIRA), Northern Arizona University, Flagstaff, AZ, 86011, USA.

*Correspondence to:

e-mail: rmendoza@materiales.unam.mx

Methodology:

a) *Reagents*. For the synthesis of Ni-Pt NPs, nickel (II) chloride hexahydrate (NiCl2 6H2O, Meyer ACS reagent), platinum (II) acetylacetonate (Pt(acac)2, Aldrich 97%), poly(diallyldimethylammonium chloride) (PDDA, Sigma-Aldrich) solution, and ethylene-glycol (EG, Meyer ≥99%) were purchased and used without further purification.

b) *Synthesis of Ni-Pt NPs*. We used a modification of a one-pot polyol method to synthesize Ni-Pt NPs with step pyramidal growth (SPNPs), using the cationic surfactant PDDA as a capping and growth directing agent. The synthesis proceeded as follows: in a 20 ml vial, NiCl2 6H2O and Pt(acac)2 (1:1 molar ratio) were dissolved and mixed in 5 ml of EG containing 200 µl PDDA at room temperature. The mixture solution was heated to 190°C for 30 minutes until the solution turned from a greenish color to a brown color, indicating the formation of particles. The colloidal solution was let to cool down at room temperature by removing the vial from the heat source. The excess of PDDA and unreacted products were removed with a mixture of ethanol/water by centrifugation at 4000 xg, allowing the resultant purified particles with sufficient molecules to stabilize them. After the process, a brown-colored solution was obtained, indicative of the NPs formation. The produced SPNPs were redispersed in water for further characterization. For Pt NPs and Ni-Pt NPs with regular shapes, the same protocol was used but without the use of PDDA as capping agent.

c) *Characterization*. The produced Ni-Pt SPNPs were mainly characterized through electron microscopy. High-resolution Scanning electron microscopy (HR-SEM) was performed in a UHR-Hitachi 5500 microscope to visualize the morphology and surface characteristics of the NPs. The crystalline structure was determined through selected-area electron diffraction (SAED) and scanning transmission electron microscopy (STEM) using a JEOL ARM-200F microscope operated at 200 keV, located at the Laboratorio Universitario de Microscopia Electrónica (LUME). The microscope is equipped with a Cescor Cs-corrector and an Aztec Oxford silicon detector for energy dispersive X-ray spectroscopy. Images were acquired in conventional transmission electron microscopy mode (TEM) and high-angle annular dark-field (HAADF) mode with convergence and collection semi-angles of 25 mrad and 68-280 mrad, respectively. For electron tomography, an image series was acquired from -65° to 65° (step 1°), and 3D-reconstructed using the simultaneous iterative reconstruction technique (SIRT) implemented in the Gatan Digital Micrograph software.[1] X-ray diffraction (XRD) measurements were performed in a Rigaku Ultima IV diffractometer using Cu K-α radiation.

d) *4-nitrophenol degradation*. The produced Ni-Pt NPs were applied in the catalytic reduction of 4-NP to 4-AP. The reaction was conducted in a 3 ml quartz cuvette, mixing 250 µl of 4-NP (1 mM) and 250 µl of $NaBH_4$ (300 mM) in 1.5 ml of water. Then, small aliquots of the Ni-Pt colloidal solution (1.47 mg/ml) or pure Pt colloidal NPs (1.47 mg/ml) were injected, monitoring the change in the UV-Vis spectrum at 400 nm. Reusability of the produced Ni-Pt NPs was studied by continuous catalytic tests. Briefly, 250 µl of $NaBH_4$ (300 mM) and 0.058 mg of Ni-Pt NPs were mixed in 1.6 ml of water. Then, 25 µl of 4-NP solution (10 mM) were injected consecutively after completing each reduction cycle, determined by the disappearance of the peak at 400 nm.

Supplementary Figures:

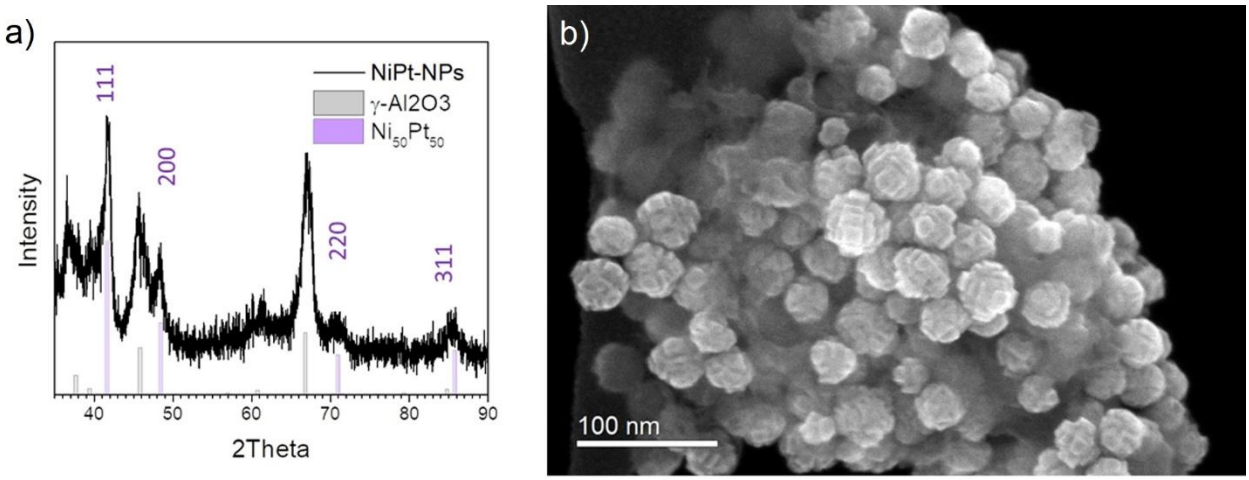

Figure S1. (a) XRD pattern of the synthesized NPs. For diffraction measurements, the samples were previously mounted on γ-Al2O3 particles by dropping the Ni-Pt colloidal solution into the support under magnetic stirring, and letting them dry entirely at 50 °C under ambient conditions. The diffraction positions corresponding to γ-Al2O3 and a Ni-Pt alloy are shown for comparison. (b) HR-SEM images of the synthesized Ni-Pt NPs. The stepped surfaces and high-index planes are observed.

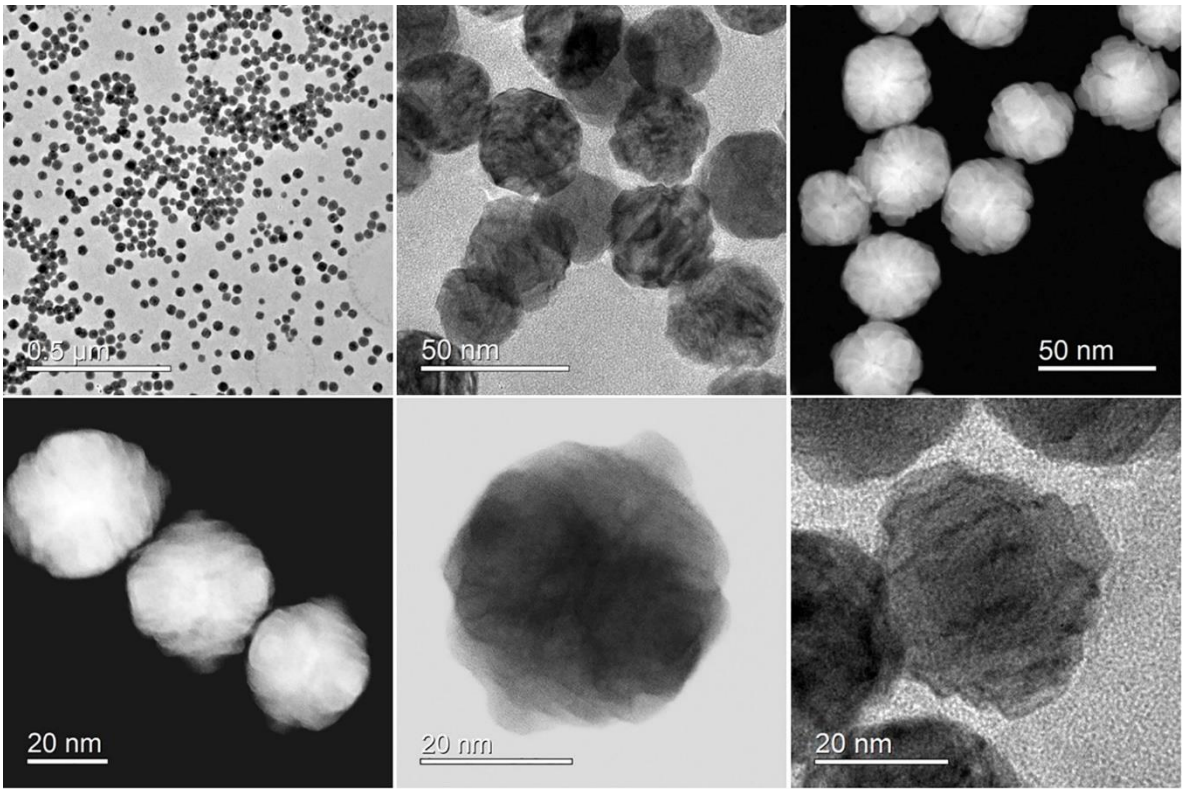

Figure S2. TEM and STEM images of the synthesized Ni-Pt NPs. The projected stepped surfaces and high-index planes are also observed.

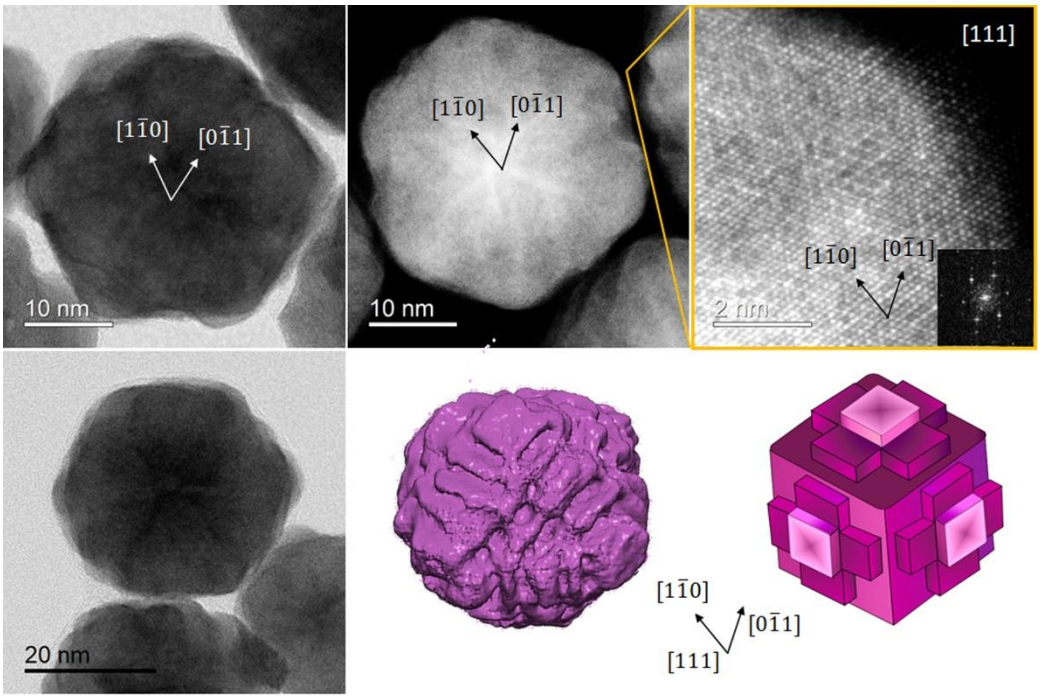

Figure S3. Top row: BF and HAADF images of single Ni-Pt NPs where the step-pyramid growth is visible. The inset corresponds to the FFT showing the single-crystal symmetry. Bottom row: Left column is a BF-STEM image of a NP oriented near the [111] zone axis. Middle column: 3D SIRT reconstruction of the NPs highlighting their stepped shape. Right column: corresponding geometrical sketch.

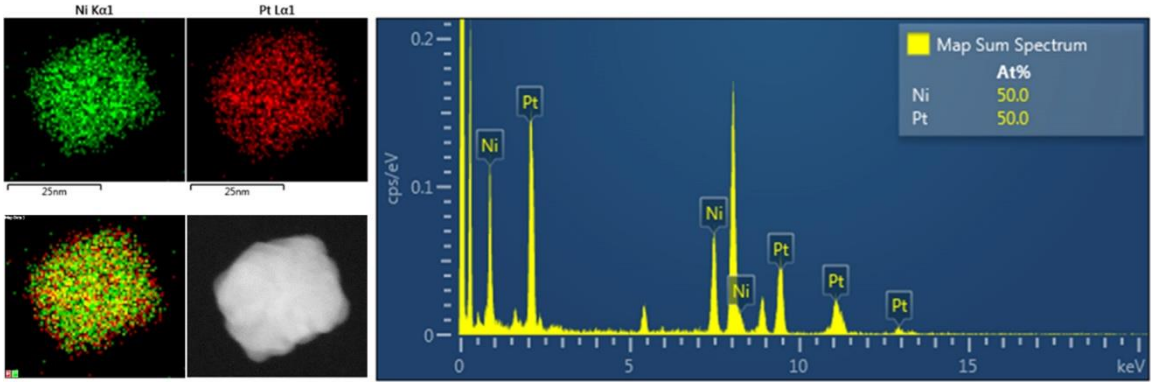

Figure S4. EDS mapping and spectrum collected from a single NP. The average atomic composition of the produced particles was Ni(49.6%) – Pt(50.4%).

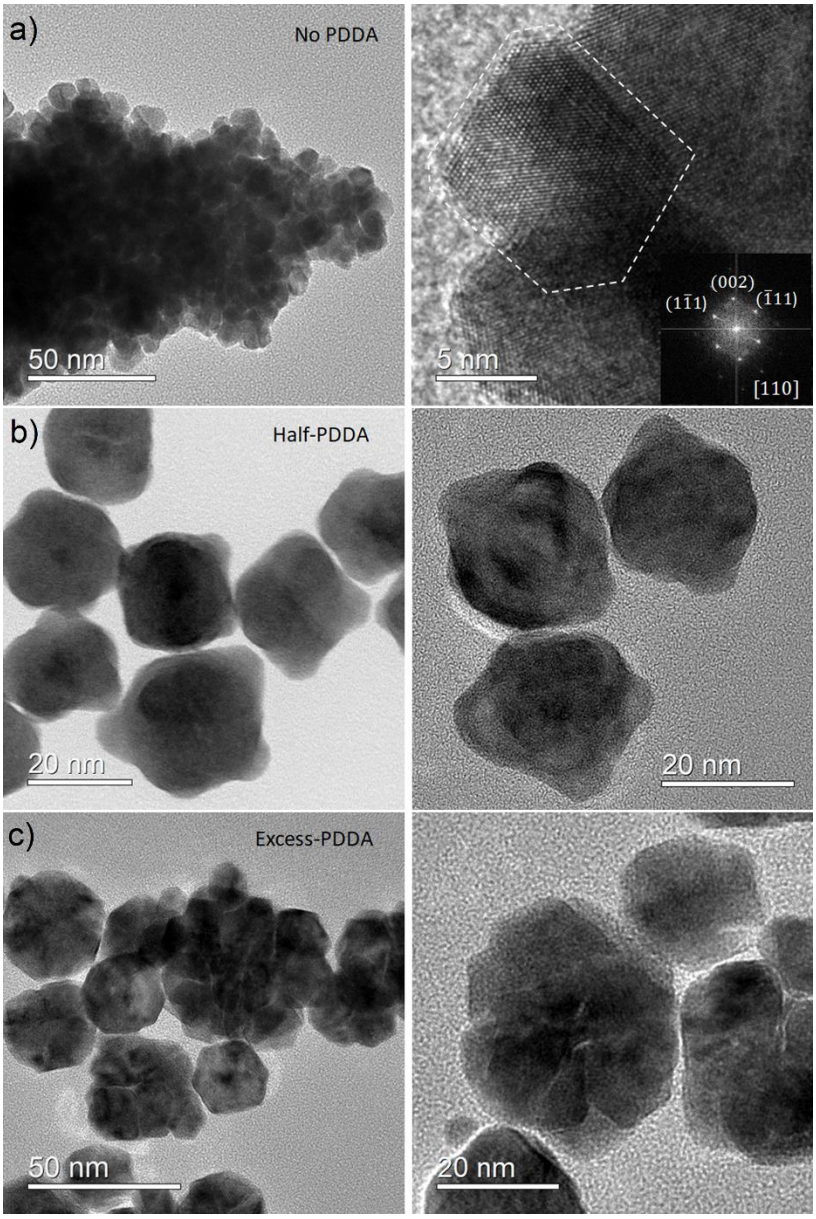

Figure S5. TEM images of particles obtained varying the amount of PDDA added to the growth solution. When no PDDA is used, small truncated octahedrons where obtained (a). Agglomeration of particles is evident due to the absence of a capping agent. When a small amount of PDDA is added (half the reported concentration), larger particles with anisotropic growth were produced with protrusions which evolved into the steps (b). When an excess of PDDA was used, more irregular particles were produced with a poor shape and size homogeneity (c).

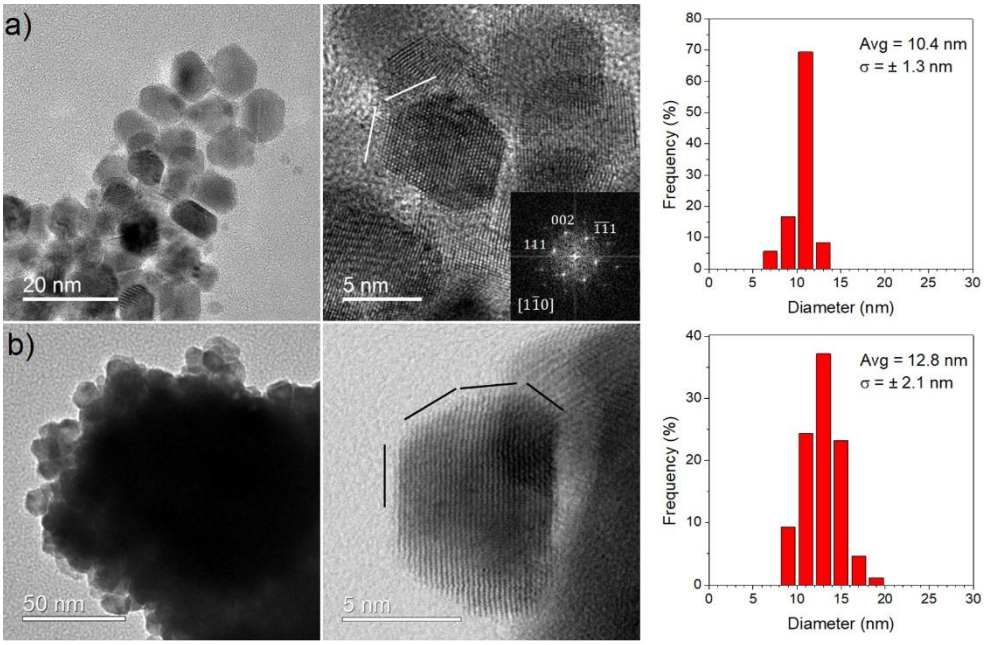

Figure S6. TEM images and size histograms of (a) Pt NPs and (b) Ni-Pt RNPs synthesized with a standard polyol method. The particles showed regular a more regular shape than SPNPs.

Catalytic reduction of 4-nitrophenol

The kinetic constant was estimated using the pseudo-first order reaction equation as follows:

$$\ln\left(\frac{C}{C_0}\right) = -kt$$

where C_0 and C are the initial concentration and the concentration of 4-NP at time t, respectively, and k is the apparent rate constant. k can be obtained from the slope in inverse units of time (s^{-1}). As the conversion rate depend on the total catalysts loading, the k/m parameter was estimated, where m is the mass in grams.

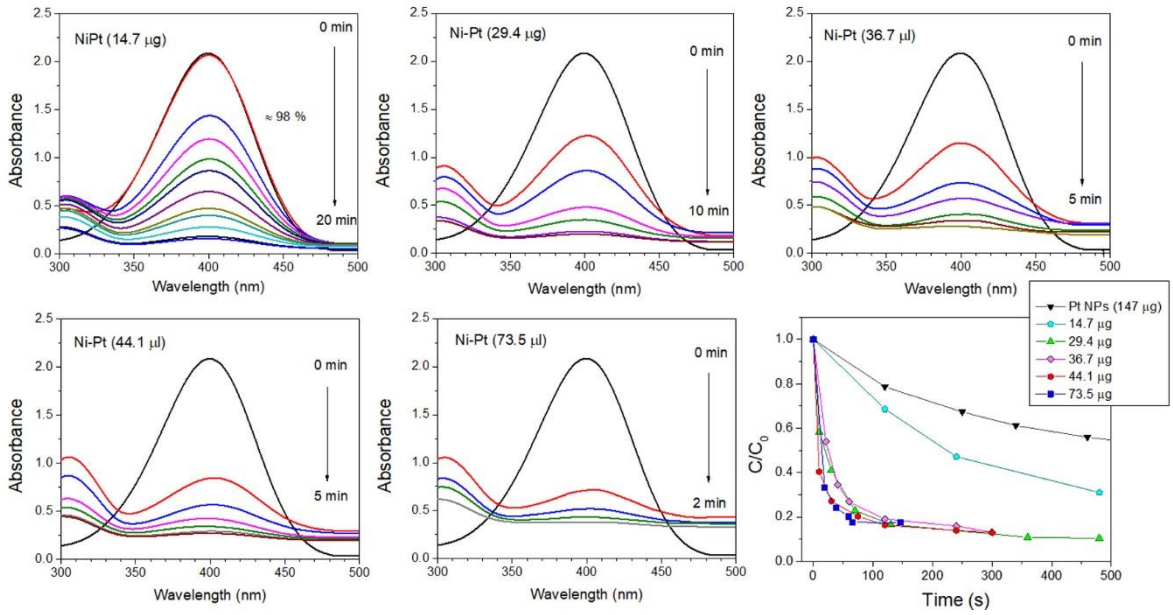

Figure S7. (a-e) Evolution of absorbance at 400 nm at different Ni-Pt NPs loading. (f) Plot C/C_0 versus each reaction time for the catalytic conversion from 4-nitrophenol to 4-aminophenol for different Pt and Ni-Pt loading.

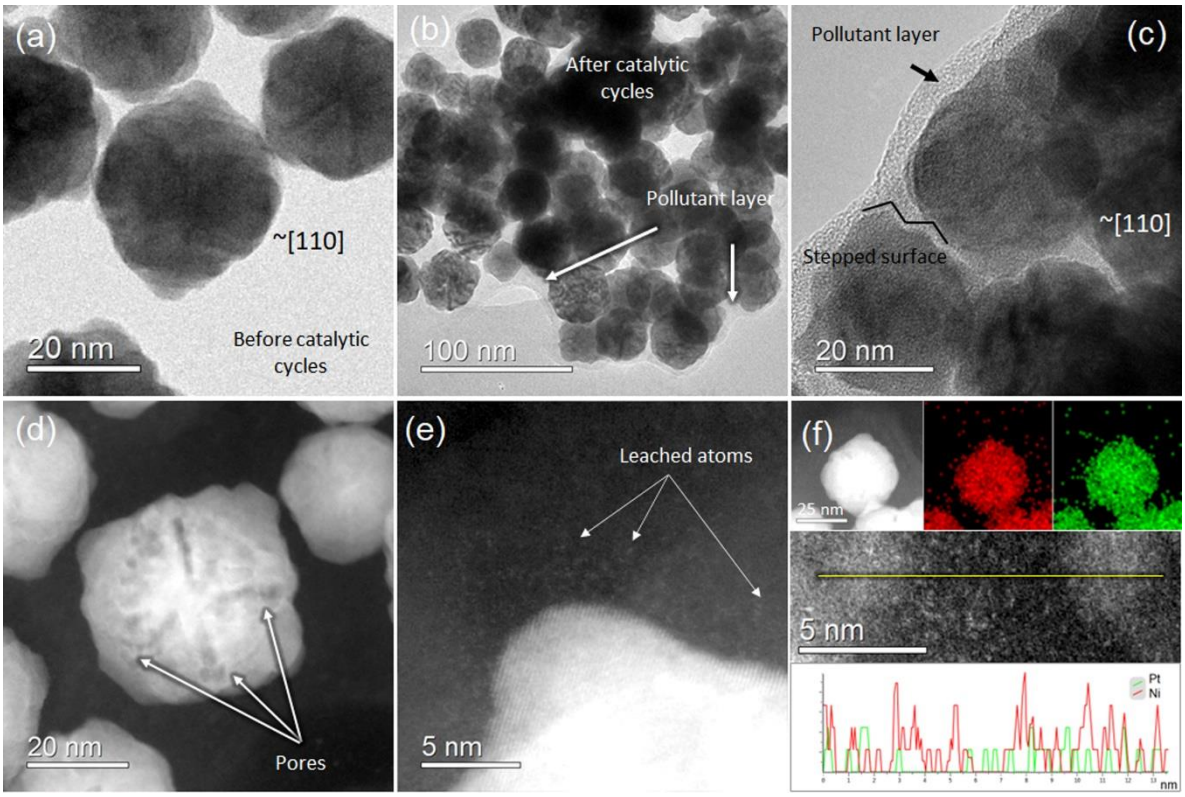

Figure S8. TEM and HAADF images of the Ni-Pt nanoparticles recovered after reusability test. (a) The particles before performing catalytic cycles oriented near the [110] zone axis. (b-e) Particles after fourteen catalytic cycles. It is observed the formation of a carbonaceous pollutant layer on the particles surface, leading to their eventual agglomeration. The general morphological features were preserved, as seen in (c,d); however, HAADF imaging in (d) enabled the visualization of pores formation due to the leaching of atoms from the metal NPs, (e). (f) EDS elemental mapping showed that the particles remained as an alloy, but with Pt and Ni atoms leached out to the surrounding layer. The average composition corresponded to Ni(51.3%)-Pt(48.7%). EDS line scan confirmed the presence of Pt and Ni into the pollutant layer.

Table S1. 4-nitrophenol reduction using unsupported and supported Pt-based nanoparticles.

Sample	Particle size (nm)	Supported	K (s^{-1})	K ($s^{-1}g^{-1}$)	Reaction time (s)	Pt content in catalyst (mg)	Cycles	Ref.
Unsupported nanostructures								
Pt NPs	6 ± 1	No	30×10^{-3}	105	100	0.286	7	[2]
Pt nanoflowers	21	No	0.7×10^{-3}	7.8	125	0.100	4	[3]
Pt-Pd NPs	4.4	No	0.53×10^{-3}	131	4800	-	6	[4]
Au-Pt/SiO_2	≈ 20	No	2.25×10^{-3}	-	1200	-	-	[5]
Pt@Ag NPs	185	No	5.9×10^{-3}	118	480	0.025	5	[6]
Pt hollow NPs	16	No	8.5×10^{-3}	-	300	-	-	[7]
Cu-Ni-Pt dendrites	10	No	11.5×10^{-3}	-	360	-	5	[8]
$Pt_{25}Co_{95}$ NPs	5.6	No	29.2×10^{-3}	146	120	0.050	4	[9]
Ni-Pt NPs	20	No	1.93×10^{-3}	483	1800	0.004	-	[10]
Ni-Pt step-pyramidal NPs	35.8	No	6×10^{-3}	427	180	0.0074	14	This work
Supported Nanostructures								
Pt NPs/CeO_2	2 - 10	Yes	4.8×10^{-3}	2.4	600	2	5	[11]
Pt-Ni NPs/RGO	10	Yes	6.2×10^{-3}	-	480	≈ 120	4	[12]
Pt_{76}-Ni_{24} NPs	2.8 – 4	Yes	-	-	300	-	6	[13]
Ni-Pt@LDH/C	11	Yes	18.8×10^{-3}	-	140	≈ 0.093	-	[14]
Pt-PDA/Fe_3O_4	50	Yes	2.3×10^{-3}	57.5	840	0.040	12	[15]
Pt NPs/Fe2O3	2.4	Yes	4×10^{-3}	-	685	≈ 0.040	10	[16]
Fe_2O_3-Pt@DSL-Pt	-	Yes	6.3×10^{-3}	-	600	-	6	[17]
Pt_3Au/RGO	26	Yes	9.6×10^{-3}	-	180	-	6	[18]
Pt-Co NDs/N-rGO	26.3	Yes	12.4×10^{-3}	1890	540	-	7	[19]
Pt/SnO_2	1.2	Yes	15.3×10^{-3}	1020	240	0.015	-	[20]
Pt/SnO_2	1.5	Yes	29.7×10^{-3}	557	120	≈0.0078	7	[21]

References

1. M. Weyland and P. Midgley, in *Transmission Electron Microscopy: Diffraction, Imaging, and Spectrometry*, eds. C. B. Carter and D. B. Williams, Springer International Publishing, Cham, 2016, DOI: 10.1007/978-3-319-26651-0_12, pp. 343-376.
2. J.-G. You, C. Shanmugam, Y.-W. Liu, C.-J. Yu and W.-L. Tseng, *Journal of Hazardous Materials*, 2017, **324**, 420-427.
3. S. Mourdikoudis, T. Altantzis, L. M. Liz-Marzán, S. Bals, I. Pastoriza-Santos and J. Pérez-Juste, *CrystEngComm*, 2016, **18**, 3422-3427.
4. Y. Tuo, G. Liu, B. Dong, H. Yu, J. Zhou, J. Wang and R. Jin, *Environmental Science Pollution Research*, 2017, **24**, 5249-5258.
5. J. Hao, B. Liu, S. Maenosono and J. Yang, *Scientific Reports*, 2022, **12**, 1-11.
6. Z.-S. Lv, X.-Y. Zhu, H.-B. Meng, J.-J. Feng and A.-J. Wang, *Journal of Colloid and Interface Science*, 2019, **538**, 349-356.
7. J. Krajczewski, K. Kołątaj and A. Kudelski, *Applied Surface Science*, 2016, **388**, 624-630.
8. H. Zhang, H. Wang, J. Cao and Y. Ni, *Journal of Alloys and Compounds*, 2017, **698**, 654-661.
9. X. Zhang, L. Chen, Y. Liu, Y. Wang and Q. Duan, *Journal of Alloys and Compounds*, 2021, **858**, 157700.
10. S. K. Ghosh, M. Mandal, S. Kundu, S. Nath and T. Pal, *Applied Catalysis A: General*, 2004, **268**, 61-66.
11. L. Zhou, X. Li, Y. Wang, M. Hong, Y. Liang and J. Zhao, *Rsc Adv*, 2014, **4**, 42965-42970.
12. F. Zhao, W. Kong, Z. Hu, J. Liu, Y. Zhao and B. Zhang, *Rsc Adv*, 2016, **6**, 79028-79036.
13. H. Ma, H. Wang and C. Na, *Applied Catalysis B: Environmental*, 2015, **163**, 198-204.
14. H. Shang, K. Pan, L. Zhang, B. Zhang and X. Xiang, *Nanomaterials*, 2016, **6**, 103.
15. S.-W. Bian, S. Liu and L. Chang, *Journal of Materials Science*, 2016, **51**, 3643-3649.
16. P. Zhang, X. Yang, H. Peng, D. Liu, H. Lu, J. Wei and J. Gui, *Catalysis Communications*, 2017, **100**, 214-218.
17. Y. Gao, J. Fang, Y. Zhang, C. Zhang, S. Zhao, Y. Zhou, M. Huang and X. Sheng, *Applied Organometallic Chemistry*, 2018, **32**, e4208.
18. W. Ye, J. Yu, Y. Zhou, D. Gao, D. Wang, C. Wang and D. Xue, *Applied Catalysis B: Environmental*, 2016, **181**, 371-378.
19. X.-F. Zhang, X.-Y. Zhu, J.-J. Feng and A.-J. Wang, *Applied Surface Science*, 2018, **428**, 798-808.
20. I. Marić, G. Dražić, E. Radin, R. Peter, M. Škrabić, T. Jurkin, A. Pustak, N. Baran, L. Mikac, M. Ivanda, M. Petravić, G. Štefanić and M. Gotić, *Applied Surface Science*, 2023, **607**, 155073.
21. S. Wu, J. Liu, Y. Ye, Z. Tian, P. Li, Y. Cai, Y. Lin and C. Liang, *Applied Surface Science*, 2019, **471**, 469-474.